Engineering of bioorthogonal polyzymes through polymer sidechain design

*Cristina-Maria Hirschbiegel †, Ritabrita Goswami †, Soham Chakraborty, Cedar Noonan, Edward Pham, Harini Nagaraj, William Ndugire, Stefano Fedeli, Vincent M. Rotello**

† The authors contributed equally to this work.

University of Massachusetts Amherst, 710 North Pleasant Street, Amherst, MA 01035, USA
* E-mail: rotello@umass.edu

Keywords: bioorthogonal catalysis, nanocatalysts, polyzymes

Abstract

Synthetic polymer scaffolds can encapsulate transition metal catalysts (TMCs) to provide bioorthogonal nanocatalysts. These 'polyzymes' catalyze the *in situ* generation of therapeutic agents without disrupting native biological processes. The design and modification of polymer scaffolds in these polyzymes can enhance the catalytic performance of TMCs in biological environments. In this study, we explore the hydrophobic design space of an oxanorborneneimide-based polymer by varying the length of its carbon side chain to engineer bioorthogonal polyzymes. Activity studies indicate that modulating the hydrophobicity of the polymer scaffold can be used to enhance the catalyst loading efficacy, catalytic activity, and serum stability of polyzymes. These findings provide insight into the structural elements contributing to improving polymeric nanocatalysts for a variety of applications.

1. Introduction

Synthetic amphiphilic polymers can self-assemble into water-soluble nanoparticles in aqueous environments.[1,2] Polymer nanoparticles have demonstrated advantageous properties for biomedical applications, such as biocompatibility, self-assembly, and high bioavailability.[3,4] Furthermore, polymer nanoparticles provide a useful scaffold for creating nanocatalysts due to their high loading capacity compared to other types of nanoparticles.[5,6] By encapsulating bioorthogonal transition metal catalysts (TMCs) into polymer nanoparticles, “polyzyme” nanocatalysts can be fabricated that transform drug precursors into active species *in situ*.[7,8] The drug precursor substrates can be synthesized by caging their therapeutically active site with a TMC-cleavable functional group.[9] The local release of the drug decreases off-target effects on healthy tissue without disturbing native bioprocesses, providing bioorthogonal “drug factories”.[10]

Polymeric encapsulation of the catalyst protects it from enzymatic degradation and deactivation in an aqueous environment, extending TMC lifetimes and improving catalytic performance.[11,12,13] Furthermore, the polymer scaffold can prevent the TMC from accessing the cytosol directly, which could induce cyto- or genotoxicity upon coordination of the free TMC with DNA and other biomacromolecules.[14]

Native enzymes use peptide architecture to provide a structured catalytic active site, achieving high catalytic turnover numbers and rates.[15] Synthetic polymers provide a design space that can be used to mimic these protein scaffolds.[16,17,18] We hypothesized that by controlling the side chain structure of the encapsulating polymer, the catalytic properties of the polyzyme could be modulated.[19,20] A hydrophobic Pd TMC was encapsulated into three different water-soluble and semi-rigid polyoxanorbornene-based (PONI) polymers featuring a systematic variation in the hydrophobicity of the side chain, yielding bioorthogonal polyzymes that catalyze the uncaging of a propargyl-caged rhodamine derivative (pro-Rho).[21, 22] Increasing the hydrophobicity of the scaffold improved the loading efficiency and, therefore, catalytic activity of the polyzymes **(Figure 1)**. Furthermore, optimizing the TMC feed ratio during polyzyme fabrication yielded polyzymes with different catalytic performance. The different polyzyme species showed varying activity loss in the presence of serum proteins, indicating that structural modifications of the polymer led to improved protection of the TMC. Overall, our results provide insight into the design of polymer nanoparticles for creating bioorthogonal nanocatalysts, highlighting the importance of the hydrophobic environment within the polymer scaffold for TMC performance.

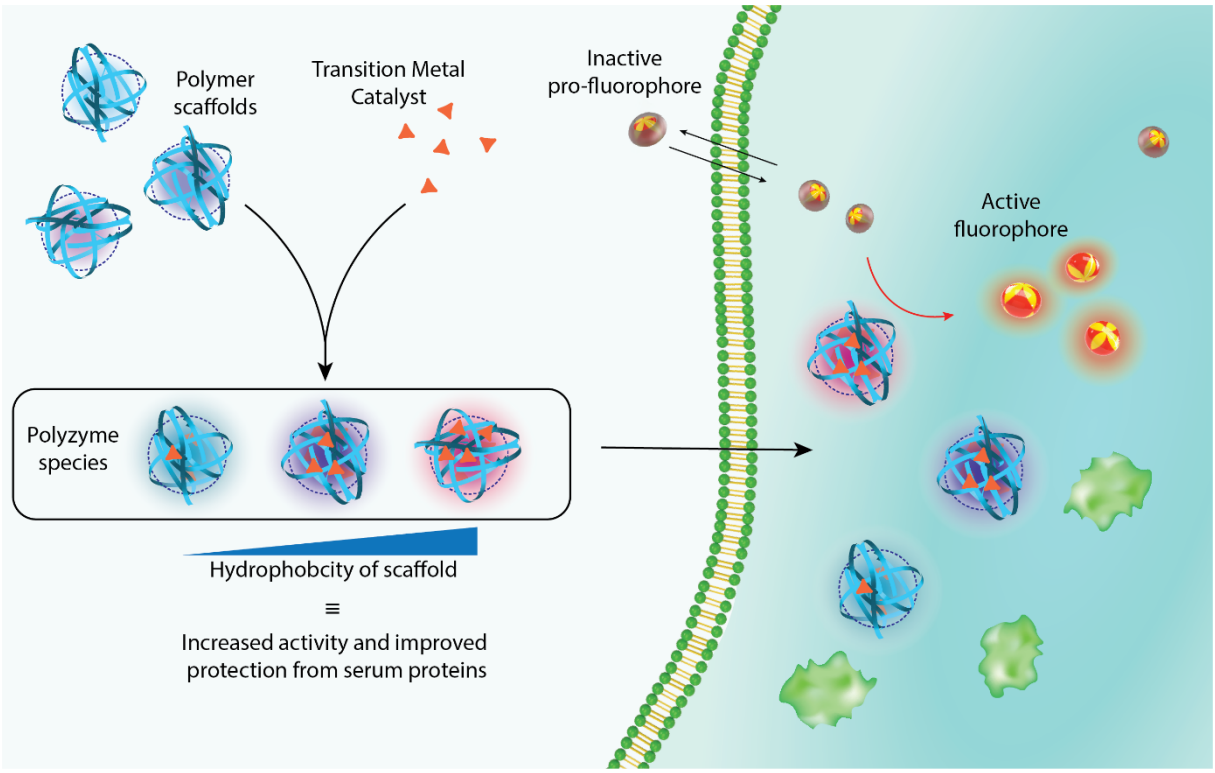

Figure 1. Polyzyme performance depends on the structure of the polymer scaffold. Increased hydrophobicity of the scaffold leads to enhanced activity and protection of the catalyst in the presence of serum proteins.

2. Results and Discussion

2.1. Polyzyme structure determines encapsulation and activity

In aqueous solutions, amphiphilic polymers self-assemble into nanoparticles bearing a hydrophobic interior and a hydrophilic exterior.[20] This arrangement provides an optimal layout for fabricating polyzymes–the hydrophobic core sequesters and protects a hydrophobic catalyst while the hydrophilic end can be functionalized for nano-bio interactions.[23,24] Previously, Huang *et al*. used an amphiphilic PONI-based scaffold featuring a lipophilic C_{11} interior and cationic trimethylamine headgroup to encapsulate iron (III) tetraphenyl porphyrin chloride, creating bioorthogonal polyzymes.[25] The cationic trimethylamine headgroup allowed the polyzyme to penetrate bacterial biofilms and efficiently uncage an antimicrobial drug locally, eradicating biofilms.

In the current study, we designed PONI-based homopolymers featuring a guanidinium (Guan) headgroup, which is preferable for use in mammalian cells due to its unique hydration properties and high biocompatibility.[26] We hypothesized that varying the carbon chain length of the linker between the backbone and the guanidinium headgroup would impact the polyzyme structure and catalysis. The polymers were synthesized from the respective monomers using

ring-opening metathesis polymerization (ROMP) polymerization, yielding PONI-C_n-Guan polymers (n = 3, 5, 7) **(Figure 2a)**. Subsequently, flash nanoprecipitation was used to encapsulate a hydrophobic Pd TMC, [1,1′-bis(diphenylphosphino)ferrocene] dichloropalladium (II), which is insoluble in water. Briefly, the respective polymer was dissolved in water, and the catalyst in acetone. The solutions were loaded into two syringes and mixed rapidly using a flash nanoprecipitation mixing chamber. The feeding ratio of the catalyst was varied for each polymer (0.5, 1.0, and 1.5 mg/mL of TMC), yielding a total of nine polyzymes **(Table 1)**. The polyzymes were characterized by DLS, indicating sizes between 10 and 30 nm for all species **(Figure S14)**. The amount of encapsulated Pd TMC was quantified using inductively coupled plasma mass spectrometry (ICP-MS) for each polyzyme **(Figure 2c)**. Significantly, increasing sidechain length increased TMC encapsulation at constant feed ratios, indicating an improvement in the loading efficiency with PONI-C_7-Guan compared to the other scaffolds. This observation can be explained by an increased hydrophobicity in the nanoparticle interior due to the carbon chain length, providing a more compatible environment for the hydrophobic catalyst. Furthermore, the loading efficiency increased with a higher feed ratio of the Pd TMC.

Table 1. Labeling system for polyzymes based on polymer structure and feed ratio of catalyst.

Feed ratio	PONI-C_3-Guan	PONI-C_5-Guan	PONI-C_7-Guan
1.5 mg/mL	C_3-1.5-PZ	C_5-1.5-PZ	C_7-1.5-PZ
1.0 mg/mL	C_3-1.0-PZ	C_5-1.0-PZ	C_7-1.0-PZ
0.5 mg/mL	C_3-0.5-PZ	C_5-0.5-PZ	C_7-0.5-PZ

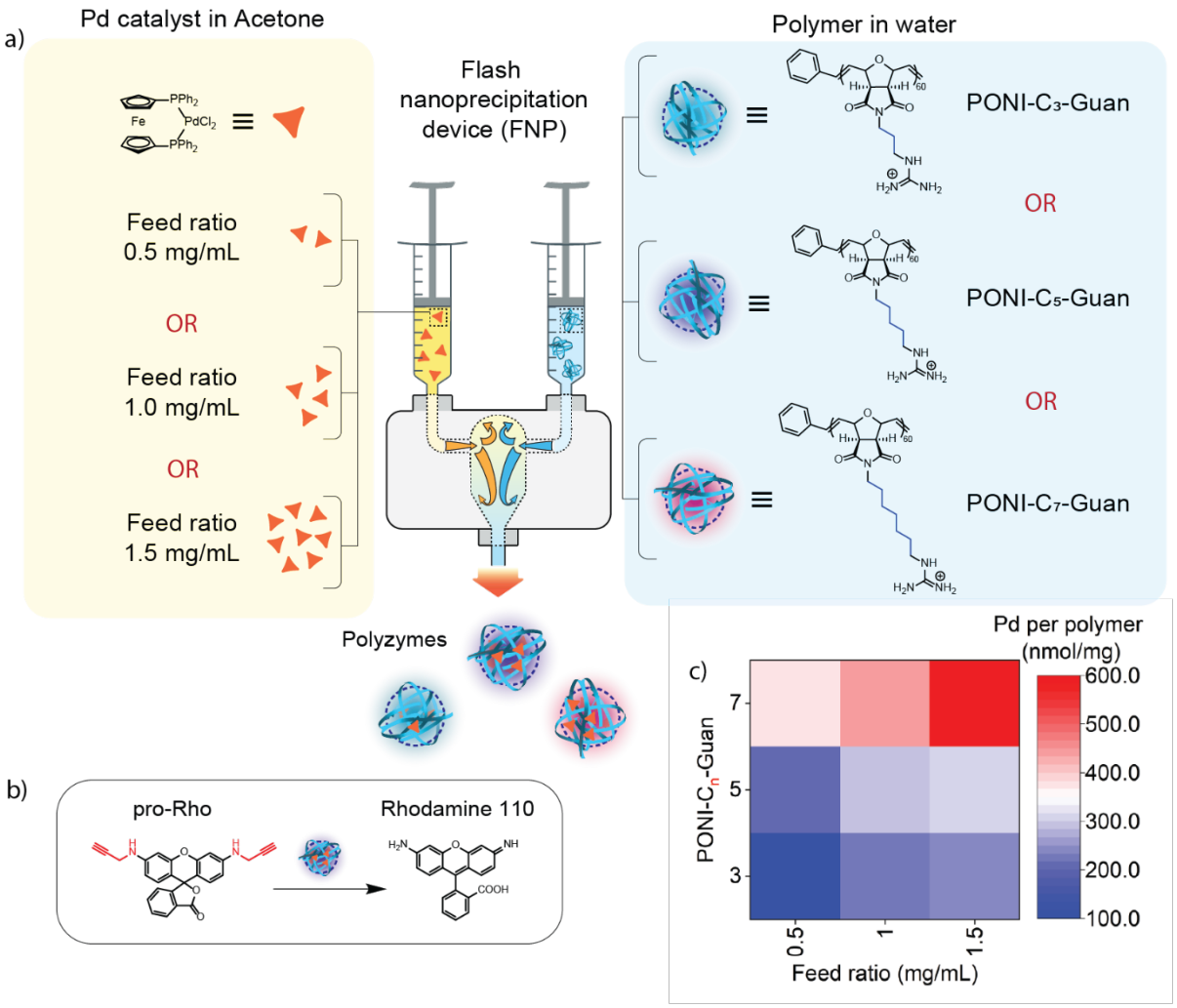

Figure 2. a) Preparation of polyzymes using varying feed ratios of Pd TMC and different PONI-C_n-Guan scaffolds, b) polyzyme catalyzed uncaging of pro-Rho to fluorescent rhodamine 110, c) quantification of Pd per polymer (nmol/mg) measured by ICP-MS.

2.2. Polymer scaffold and TMC feed ratio determine catalytic performance

The encapsulated Pd TMC catalyzes the uncaging of a propargyl-caged rhodamine 110 derivative (pro-Rho), releasing fluorescent rhodamine 110 **(Figure 2b)**.[11] The fluorophore release was monitored by fluorescence spectroscopy (ex. 488 nm, em. 521 nm) **(Figure 3)**. The polyzymes of different polymer species with a constant feed ratio of 1.0 mg/mL were compared to each other to understand the effect of the scaffold on the catalytic performance of the polyzyme **(Figure 3a)**. The polyzyme species based on PONI-C_7-Guan (C_7-1.0-PZ) achieved significantly more uncaging than the polyzyme fabricated using PONI-C_3-Guan (C_3-1.0-PZ). Furthermore, C_5-1.0-PZ and C_7-1.0-PZ showed similar pro-Rho activation in the first 30 minutes of catalysis, but the fluorophore release of C_5-1.0-PZ slowed down and reached a plateau considerably earlier than C_7-1.0-PZ. These results agree with the increase in TMC

encapsulation driven by the hydrophobicity of the scaffold, as observed by ICP-MS **(Figure 2c)**.

We next performed the pro-Rho activation using the same scaffold (PONI-C_7-Guan) but varying the feed ratio of the Pd TMC **(Figure 3b)**. Hypothetically, an increased catalyst loading at higher feed ratios of TMC should reflect an improved catalytic performance, as observed with the different polymer scaffolds. However, when maintaining the same polymer scaffold at different feed ratios, the PONI-C_7-Guan-based polyzymes demonstrated a significantly better performance at a 1 mg/mL feed ratio of Pd TMC as opposed to either 0.5 and 1.5 mg/mL feed ratios. Similar results were observed using the PONI-C_3- and PONI-C_5-Guan-based polyzymes **(Figure S17)**. These results indicate that more catalyst within the polymer scaffold does not necessarily lead to a better performance of the polyzyme but instead that an optimum loading amount exists, providing easy substrate access to the TMC.

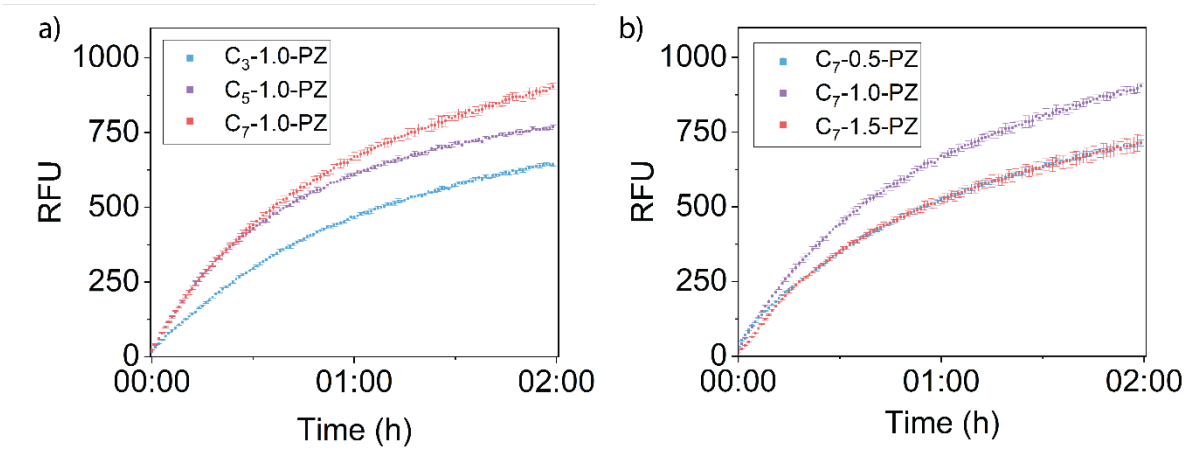

Figure 3. Reaction kinetics of a) different polyzyme species at constant feed ratio (1.0 mg/mL Pd TMC) and b) polyzymes fabricated using PONI-C_7-Guan with varying feed ratio (0.5/1.0/1.5 mg/mL Pd TMC).

We next performed the fluorophore release using the respective polyzyme in PBS containing 10% fetal albumin serum (FBS) to observe changes in the catalytic activity in the presence of serum proteins while using the same substrate and polyzyme concentrations as in the serum-free kinetics **(Figure S20a-c)**. A decrease in activity for all species was observed. This observation can be explained by the formation of a protein corona around cationic nanoparticles, as previously observed in the literature.[11] Cationic nanoparticles interact through charge-charge interactions with the negatively charged surface of serum proteins, significantly decreasing the accessibility of the substrate to the catalyst.[12,13] The loss in activity was determined by comparing the catalytic fluorophore uncaging after 30 min of the reaction at the same concentrations of pro-Rho and polyzyme in PBS and 10% FBS **(Figure S20d)**. While C_3-

1.0-Guan and C_5-1.0-Guan showed a significant activity loss (70% and 67%, respectively), C_7-1.0-Guan showed less loss of activity (59%) in serum-containing PBS. These results indicate improved protection of the TMC due to the polymer scaffold and increased encapsulation.

2.3. Comparison of Michaelis-Menten kinetics of PONI-C_7-Guan polyzymes

Michaelis-Menten enzyme kinetics provide insight into the enzyme performance and binding affinity of the substrate to the enzyme and can be applied to understand the behavior of bioorthogonal polyzymes. We incubated the PONI-C_7-Guan-based polyzymes with different substrate concentrations of pro-Rho at 37 °C in PBS, maintaining the same polyzyme concentration. Thereafter, we calculated the respective Michaelis-Menten constants (K_m) and catalytic constant (K_{cat}) of the polyzymes **(Furthermore,** the C7-1.5-PZ shows the largest amount of encapsulated catalyst compared to the other polyzyme species **(Figure 2c)** and the largest size according to DLS compared to the PONI-C7-Guan-based polyzymes. Despite these findings, C7-1.5-PZ performs the pro-dye transformation less efficiently than C7-1.0-PZ **(**

Figure *4c*), indicating catalyst clustering within the nanoscaffold.

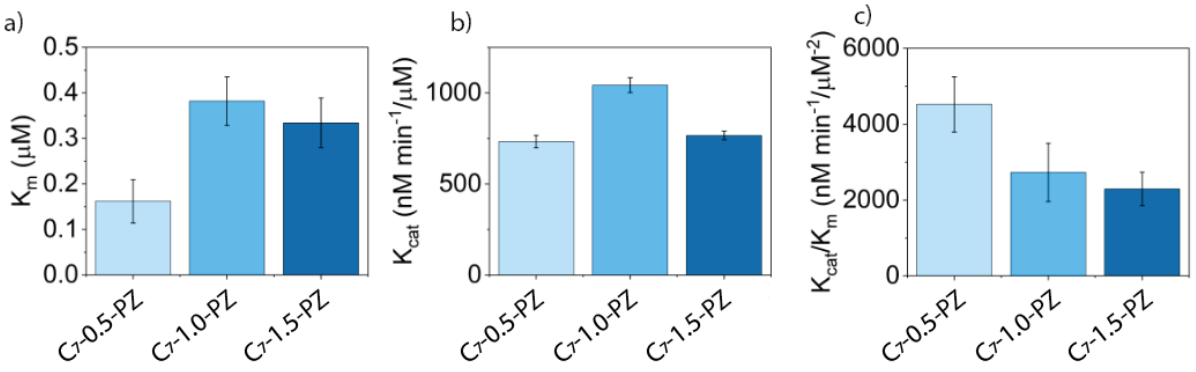

Figure *4a* and **b, Table S1** and **S2, Figure S19)**. In agreement with our previous kinetics experiment **(Figure 3b)**, C_7-1.0-PZ possessed a higher K_m and K_{cat} than C_7-0.5- and C_7-1.5-PZ, indicating improved polyzyme performance at a feed ratio of 1.0 mg/mL of Pd TMC. These results align with our hypothesis that at a 1.0 mg/mL feed ratio, the catalytic sites within the polyzymes are sufficient and accessible to the substrate. Within the group of polyzymes fabricated using PONI-C_7-Guan, we observed a higher K_{cat}/K_m ratio for the polyzyme fabricated with the lowest feed ratio of catalyst (0.5 mg/mL), indicating more efficient catalysis **(**

Figure *4c*).[27] In fact, C_7-0.5-PZ performed the catalytic release of Rho 110 at low substrate concentration (0.5 and 1 uM) at a similar velocity as C_7-1.0-PZ **(Figure S18)**, indicating facile substrate access at low occupancy of the catalyst molecules within the scaffold. At higher

loading of the TMC, the polyzyme efficiency decreases. This phenomenon could occur due to less access of the substrate to the catalyst molecules within the scaffold, which can be explained by steric hindrance resulting from catalyst clustering or steric blockage of the polymer.[28] These observations can be related to the smaller size of the C_7-1.0-PZ measured by DLS coupled with increased catalyst density **(Figure S14)** and, therefore, a more constrained environment. Furthermore, the C_7-1.5-PZ shows the largest amount of encapsulated catalyst compared to the other polyzyme species **(Figure 2c)** and the largest size according to DLS compared to the PONI-C_7-Guan-based polyzymes. Despite these findings, C_7-1.5-PZ performs the pro-dye transformation less efficiently than C_7-1.0-PZ **(**

Figure *4*c), indicating catalyst clustering within the nanoscaffold.

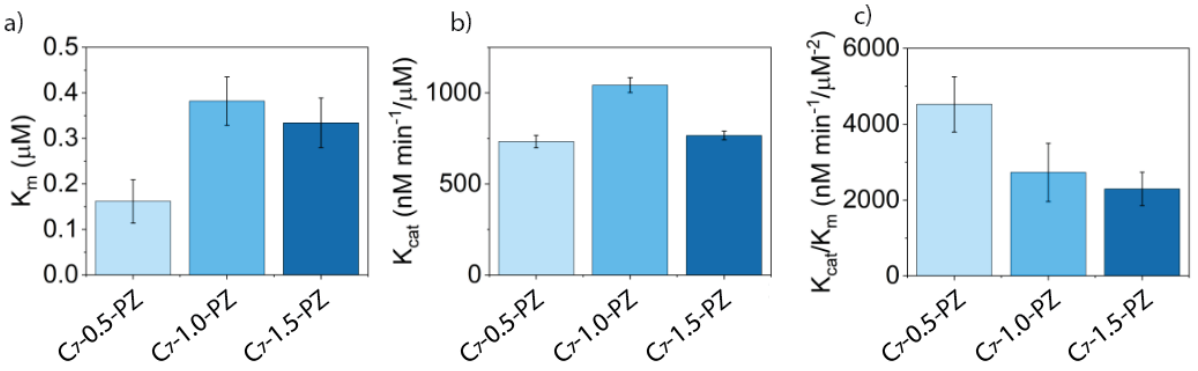

Figure 4. a) K_m, b) K_{cat}, and c) K_{cat}/K_m values of PONI-C_7-Guan-based polyzymes with respective error bars.

2.4. Activation of fluorophores in HeLa cells

Having evaluated the catalytic activity of the PONI-C_7-Guan-based polyzymes in solution, we explored their catalytic efficacy in cancer cells. As a proof of concept, the fluorophore release was performed in HeLa cells using C_7-1.0-PZ. HeLa cells were treated with the polyzyme (300 nM) and pro-Rho (50 μM) for 24 h, and the resulting fluorescence was monitored using a confocal microscope **(Figure 5)**. No green fluorescence was observed in cells treated with pro-Rho or the polyzyme alone. These results demonstrate the translatability and biocompatibility of the fabricated polyzyme.

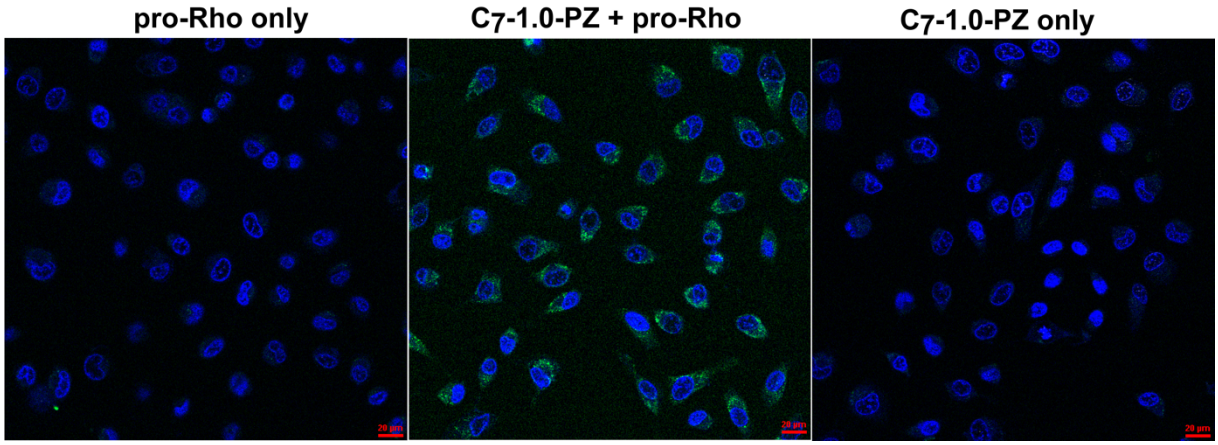

Figure 5. Confocal microscopy images of HeLa cells incubated with 300 nM of C_7-1.0-PZ and 50 μM pro-Rho. Nuclei were stained by Hoechst 33342. Scale bars, 20 μm.

3. Conclusion

In summary, we have demonstrated that by modifying the polymer scaffold used for polyzyme fabrication, the loading efficiency of the TMC can be improved. Furthermore, modifying the scaffold leads to variations in the catalytic activity of the resulting polyzyme. By increasing the hydrophobicity of the polymer scaffold, an improvement in the catalytic efficacy and prolonged activity of the TMC in a serum-containing environment can be observed. Furthermore, previous studies performed by Paulusse and co-workers have highlighted the importance of the hydrophobic design of nanomaterials for cell permeation, paving the way for future studies of polyzyme design on cellular uptake.[29] Our results directly correlate the structure of the polymer scaffold with the catalytic activity of polyzymes. Thereby, our findings provide an understanding of the structural elements that participate in improving the design of polyzymes, paving the way for the future design of polymeric nanocatalysts.

4. Experimental Section/Methods

Polymer synthesis and characterization: PONI backbone C_3-guanidinium (Guan) monomers were prepared as previously described.[22, 30, 31] The C_5- and C_7-Guan monomers were synthesized similarly by using tert-Butyl (5-bromopentyl)carbamate and tert-Butyl (7-bromoheptyl)carbamate, respectively, in the first step as described in the previous protocols. A detailed protocol and characterization of the C_5 and C_7 monomers can be found in the supporting information **(Figure S1-6)**. Homopolymers were synthesized by ring-opening metathesis polymerization (ROMP) using a third-generation Grubbs' catalyst, and the degree of polymerization was kept constant at 60. In brief, both solutions of guanidium functionalized monomer and Grubbs' catalyst in DCM were placed under freeze-thawing cycles for degassing.

After warming the solutions to room temperature, the degassed monomer solutions were administrated to degassed catalyst solutions and stirred for 20 min. The addition of excess ethyl vinyl ether terminated the polymerization reaction. The reaction mixture was stirred for another 30 min. The resultant polymers were precipitated from excess hexane, diethyl ether anhydrous, or cold methanol, filtered, washed, and dried under vacuum to yield a light-yellow powder. The reaction yields varied from 90% to 98%. All polymers were characterized by ^{1}H NMR **(Figure S7-12)** and gel permeation chromatography (GPC) to assess chemical compositions and molecular weight distributions, respectively **(Figure S13)**. After the deprotection of Boc functionalities, the polymer was dissolved in the DCM with the addition of TFA at a 1:1 ratio. The reaction was allowed to stir for 4 hours and dried under vacuum. Excess TFA was removed by azeotropic distillation with methanol. Afterward, the resultant polymers were re-dissolved in DCM, precipitated in anhydrous diethyl ether, filtered, washed, and dried. Polymers were then dissolved in water, transferred to Biotech CE dialysis tubing membranes with a molecular weight cut-off of 10,000 g/mol, and dialyzed against MQ water (2−3 days). The polymers were then lyophilized to yield a light white powder.

Polyzyme fabrication: Polyzymes were fabricated using flash nanoprecipitation (FNP) according to previous protocols.[32] Briefly, the Pd TMC was dissolved in acetone at different concentrations (0.5, 1.0, and 1.5 mg/mL), and the respective polymer was dissolved in water (1 mg/mL). Of the respective solutions, 0.6 mL were loaded into two separate 1 mL syringes and attached to an FNP mixing chamber. After that, the solutions were rapidly pushed into the mixing chamber (<1 sec) and led into a rapidly stirring 6 mL MQ water quench bath. The resulting solution was stirred for approximately 2 minutes before being transferred into a centrifuge filter (30K MW cut-off), where it was centrifuged and washed with MQ water 3 times (2800 rpm, 8 min, 23 °C). The polyzyme solution was transferred out of the centrifuge filter and filtered through a 0.45 μm Nylon syringe filter. The mass of the solution was taken to calculate the final concentration of the polyzymes based on the weight of the initially used polymer. The size of the respective polyzymes was determined using DLS **(Figure S14)**. The amount of encapsulated Pd TMC per mg of polymer was determined using ICP-MS **(Figure S15, Table S1)**.

Kinetics of fluorophore release: We performed the uncaging of pro-Rho using the respective polyzymes and the same conditions for each experiment. Briefly, in a 96-well plate at 37 °C, 50 μL of the polyzyme solution and 50 μL of the pro-Rho solution were combined, reaching final concentrations of 0.05 mg/mL and 8 μM, respectively. The stock solution of pro-Rho was

prepared in DMSO and diluted with MQ water to reach a final DMSO content of less than 2%. Negative controls contained either the respective polyzyme or the pro-Rho at the same concentrations used in the experiment. The fluorophore release was monitored over 2 h using a spectral photometer and measuring the fluorescence of the product (ex. 488 nm, em. 521 nm). Each experiment was performed in triplicate.

Michaelis-Menten kinetics: Michaelis-Menten kinetics were performed similarly to the kinetics of the fluorophore release described above. Briefly, in a 96-well plate at 37 °C, 50 µL of the polyzyme solution (final concentration of 0.05 mg/mL) and 50 µL of the pro-Rho solution were combined, with varying concentrations of pro-Rho (0.5/1/2/4/8 µM) for each respective polyzyme. The fluorophore release was monitored over 20 min using a spectral photometer and measuring the fluorescence of the product (ex. 488 nm, em. 521 nm). Each experiment was performed in triplicate. The resulting relative fluorescence units were transformed into substrate concentration using a standard curve **(Figure S16)** and plotted against time using the software Origin Pro 7.0. The slopes of the respective curves were calculated and plotted against the substrate concentration. From this data, the K_m and v_{max} values were calculated using the Michael-Menten non-linear curve fitting embedded in the software **(Figure S17, Table S2)**. The catalytic constant K_{cat} was calculated from v_{max} divided by the enzyme concentration.

Cell culture and confocal microscopy: HeLa cells (ATCC CCL-2) were used for cytotoxicity and imaging experiments. For the cytotoxicity assay, 1.0 x 10^4 cells/well were seeded in 96-well plates 24 h prior to the experiment. For the imaging experiment, 20 x 10^4 cells/well were seeded in 35 mm round confocal dishes (Mattek) 24 h prior to the experiment. The cells were cultured in Dulbecco's modified Eagle medium (DMEM; ATCC 30-2002) with 10% bovine fetal serum and 1% antibiotics at 37 ºC in a humidified atmosphere of 5% CO2 for 24 h. The cell viability was determined using Alamar Blue assay according to the manufacturer's protocol (Invitrogen), using Molecular Devices Spectramax M2 and SoftMax Pro 7 software.

Confocal microscopy imaging experiments were performed using a Nikon TiE stand with an A1 Spectral Detector Confocal and a FLIM/FCS Module. Cell staining was performed 20 min before imaging with Hoechst 33,342 solution (Thermofisher, Waltham, MA, USA) to visualize nuclei.

Supporting Information

Supporting Information is available from the Wiley Online Library or from the author.

Acknowledgements

This research was funded by the National Institutes of Health R01 EB022641 (V.M.R.). C.-M.H. was partially supported by a fellowship from the University of Massachusetts as part of the Chemistry-Biology Interface Training Program (National Research Service Award T32 GM139789). W. N. was partially supported by EB022641-S. C.-M. H. and R. G. contributed equally to this work.

Received: ((will be filled in by the editorial staff))
Revised: ((will be filled in by the editorial staff))
Published online: ((will be filled in by the editorial staff))

[1] E. Krieg, M. M. C. Bastings, P. Besenius, B. Rybtchinski, *Chem. Rev*. **2016**, *116*, 2414-2477

[2] G. J. Gabriel, A. Som, A. E. Madkour, T. Eren, G. N. Tew, *Mater. Sci. Eng.: R: Rep*. **2007**, *57*, 28-64

[3] S. Fedeli, J. Im, S. Gopalakrishnan, J. L. Elia, A. Gupta, D. Kim, V. M. Rotello, Chem. Soc. Rev. **2021**, *50*, 13467-13480

[4] M. J. Mitchell, M. M. Bilingsley, R. M. Haley, M. E. Wechsler, N. A. Peppas, R. Langer, Nat. Rev. Drug Discovery **2021**, *20*, 101-124

[5] R. Huang, C.-M. Hirschbiegel, V. Lehot, L. Liu, Y. A. Cicek, V. M. Rotello, *Adv. Mater*. **2023**. Accepted Author Manuscript, 2300943. https://doi.org/10.1002/adma.202300943

[6] J. Miguel-Ávila, M. Tomás-Gamasa, J. L. Mascareñas, *Trends Chem*. **2023**. *5*, 474-485

[7] C.-M. Hirschbiegel, S. Fedeli, X. Zhang, R. Huang, J. Park, Y. Xu, V. M. Rotello, *Materials* **2022**, *15*, 6487

[8] X. Zhang, R. F. Landis, P. Keshri, R. Cao‐Milán, D. C. Luther, S. Gopalakrishnan, Y. Liu, R. Huang, G. Li, M. Malassiné, I. Uddin, B. Rondon, V. M. Rotello, *Adv. Healthcare Mater*. **2020**, *10*, 2001627

[9] T. Liang, Z. Chen, H. Li, Z. Gu, *Trends Chem*. **2022**, *4*, 157-168

[10] X. Zhang, Y. Liu, J. Doungchawee, L. J. Castellanos-García, K. N. Sikora, T. Jeon, R. Goswami, S. Fedeli, A. Gupta, R. Huang, C.-M. Hirschbiegel, R. Cao-Milán, P. K. D. Majhi, Y. A. Cicek, L. Liu, D. J. Jerry, R. W. Vachet, V. M. Rotello, *J. Controlled Release* **2023**, *357*, 31-39

[11] X. Zhang, S. Fedeli, S. Gopalanrishnan, R. Huang, A. Gupta, D. C. Luther, V. M. Rotello, *ChemBioChem* **2020**, *21*, 2759-2763

[12] K. Saha, D. F. Moyano, V. M. Rotello, *Mater. Horiz*. **2014**, *1*, 102-105

[13] X. Zhang, Y. Liu, S. Gopalakrishnan, L. Castellanos-Garcia, G. Li, M. Malassine, I. Uddin, R. Huang, D. C. Luther, R. W. Vachet, V. M. Rotello, *ACS Nano* **2020**, *14*, 4767-4773

[14] Y. Bai, J. Chen, S. C. Zimmerman, *Chem. Soc. Rev*. **2018**, *47*, 1811-1821

[15] A. Sharma, G. Gupta, T. Ahmad, S. Mansoor, B. Kaur, *Food Rev. Int*. **2021**, *37*, 121-154

[16] J. P. Cole, A. M. Hanlon, K. J. Rodrigues, E. B. Berda, *J. Polym. Sci., Part A: Polym. Chem*. **2016**, *55*, 191-206

[17] G. M. Ter Huurne, A. R. A. Palmans, E. W. Meijer, *CCS Chem*. **2019**, *1*, 64-82

[18] J. Chen, J. Wang, Y. Bai, K. Li, E. S. Garcia, A. L. Ferguson, S. C. Zimmerman, *J. Am. Chem. Soc.* **2018**, *140*, 13695-13702

[19] E. Huerta, B. Van Genabeek, B. A. G. Lamers, M. M. E. Koenigs, E. W. Meijer, A. R. A. Palmans, *Chem. Eur. J.* **2015**, *21*, 3682-3690

[20] S.-Y. Huang, C.-C. Cheng, *Nanomaterials* **2020**, *10*, 10102006

[21] C. R. Hango, H. C. Davis, E. A. Uddin, L. M. Minter, G. N. Tew, *Polym. Chem*. **2022**, *13*, 1901-1910

[22] T. Jeon, D. C. Luther, R. Goswami, C. Bell, H. Nagaraj, Y. A. Cicek, R. Huang, J. A. Mas-Rosaio, J. L. Elia, J. Im, Y.-W. Lee, Y. Liu, F. Scaletti, M. E. Farkas, J. Mager, V. M. Rotello, *ACS Nano* **2023**, *17*, 4315-4326

[23] S. A. Dergunov, A. T. Khabiyev, S. N. Shmakov, M. D. Kim, N. Ehterami, M. C. Weiss, V. B. Birman, E. Pinkhassik, *ACS Nano* **2016**, *10*, 11397-11406

[24] C. Boucher-Jacobs, M. Rabnawaz, J. S. Katz, R. Even, D. Guironnet, *Nat. Comm*. **2018**, *9*, 841

[25] R. Huang, C.-H. Li, R. Cao-Milán, L. D. He, J. M. Makabenta, X. Zhang, E. Yu, and V. M. Rotello, *J. Am. Chem. Soc*. **2020**, *142*, 10723–10729

[26] P. E. Mason, G. W. Neilson, C. E. Dempsey, A. C. Barnes, J. M. Cruickshank, *PNAS* **2003**, *100*, 4557-4561

[27] D. E. Koshland Jr. *Bioorg. Chem*. **2002**, *30*, 211-213

[28] R. Cao-Milan, S. Gopalakrishnan, L. D. He, F. Scaletti, R. W. Vachet, V. M. Rotello, *Chem* **2020**, *6*, 1113-1124

[29] N. M. Hamelmann, J.-W. D.Paats, J. M. J. Paulusse, *ACS Macro Lett*. **2021**, 10, 1443–1449

[30] Y.-W. Lee, D. C. Luther, R. Goswami, T. Jeon, V. Clark, J. Elia, S. Gopalakrishnan, V. M. Rotello, *J. Am. Chem. Soc*. **2020**, *142*, 4349-4355

[31] R. Goswami, V. Lehot, Y. A. Cicek, H. Nagaraj, T. Jeon, T. Nguyen, S. Fedeli, V. M. Rotello, *Pharmaceutics* **2023**, *15*, 218

[32] R. Huang, C.-M. Hirschbiegel, X. Zhang, A. Gupta, S. Fedeli, Y. Xu, V. M. Rotello, *ACS Appl. Mater. Interfaces* **2022**, *14*, 31594–31600